Biosensors and Bioelectronics 39 (2013) 1–13

Contents lists available at SciVerse ScienceDirect

Biosensors and Bioelectronics

journal homepage: www.elsevier.com/locate/bios

Cytochrome P450 (CYP) enzymes and the development of CYP biosensors

Elizabeth Schneider, Douglas S. Clark*

Department of Chemical and Biomolecular Engineering, University of California, Berkeley 201 Gilman Hall, Berkeley, CA 94720, USA

ARTICLE INFO

Article history:
Received 19 March 2012
Received in revised form
29 May 2012
Accepted 30 May 2012
Available online 26 June 2012

Keywords:
Cytochrome P450
CYP
Biosensor
Enzyme electrode
Bioelectrochemistry

ABSTRACT

Cytochrome P450s (CYPs) are a large family of heme-containing monooxygenase enzymes involved in the first-pass metabolism of drugs and foreign chemicals in the body. CYP reactions, therefore, are of high interest to the pharmaceutical industry, where lead compounds in drug development are screened for CYP activity. CYP reactions in vivo require the cofactor NADPH as the source of electrons and an additional enzyme, cytochrome P450 reductase (CPR), as the electron transfer partner; consequently, any laboratory or industrial use of CYPs is limited by the need to supply NADPH and CPR. However, immobilizing CYPs on an electrode can eliminate the need for NADPH and CPR provided the enzyme can accept electrons directly from the electrode. The immobilized CYP can then act as a biosensor for the detection of CYP activity with potential substrates, albeit only if the immobilized enzyme is electroactive. The quest to create electroactive CYPs has led to many different immobilization strategies encompassing different electrode materials and surface modifications. This review focuses on different immobilization strategies that have been used to create CYP biosensors, with particular emphasis on mammalian drug-metabolizing CYPs and characterization of CYP electrodes. Traditional immobilization methods such as adsorption to thin films or encapsulation in polymers and gels remain robust strategies for creating CYP biosensors; however, the incorporation of novel materials such as gold nanoparticles or quantum dots and the use of microfabrication are proving advantageous for the creation of highly sensitive and portable CYP biosensors.

Contents

Abbreviations: PSS, poly(styrenesulfonate); PDDA, poly(dimethyldiallylammonium chloride); MPS, mercaptopropenesulfonic acid; PEI, poly(ethylenimine); CPR, cytochrome P450 reductase; DDAB, didodecyldimethylammonium bromide; DMPC, L-α-phosphatidylcholine dimyristoyl; NNK, 4-(methylnitrosamino)-1-(3-pyridyl)-1-butanone; HPB, 4-hydroxy-1-(3-pyridyl)-1-butanone; BSA, bovine serum albumin; EDC, 1-Ethyl-3-[3-dimethylaminopropyl]carbodiimide hydrochloride; NHS, N-hydroxysuccinimide; OT, octanethiol; MUA, 11-mercaptoundecanoic acid; 6HT, 6-hexanethiol; 7MHA, 7-mercaptoheptanoic acid; MPA, mercaptopropionic acid; DTME, dithio-bismaleimidoethane; MWCNTs, multi-walled carbon nanotubes

* Corresponding author. Tel.: +1 510 642 2408.
E-mail address: clark@berkeley.edu (D.S. Clark).

0956-5663/$ - see front matter © 2012 Elsevier B.V. All rights reserved.
http://dx.doi.org/10.1016/j.bios.2012.05.043

1. Introduction

Cytochrome P450s (CYPs) are a family of heme-containing enzymes implicated in the metabolism of xenobiotics in the body. Five CYPs (CYP1A2, 2C9, 2C19, 2D6, and 3A4) are responsible for approximately 95% of CYP-mediated drug metabolism in the body (Williams et al., 2004), with the remaining CYP enzymes being involved in steroidogenesis and fatty acid oxidation. CYPs catalyze the hydroxylation, epoxidation, and N-, S-, and O-demethylation of drug molecules, allowing for second-phase metabolism and excretion from the body. Consequently, P450 reactions are of high interest to the pharmaceutical industry, where lead compounds in drug development are screened as potential substrates or inhibitors of CYPs. Knowing the P450 substrate profile of a drug allows for the prediction of harmful drug–drug or food–drug interactions, which are often caused by the interference of CYP metabolism via inhibition or induction of a specific P450 isozyme.

Currently, the development of screens for CYP activity against drug candidates is hindered by the lack of methods that match the throughput achieved in other steps of the drug development process such as combinatorial library generation (Ansede and Thakker, 2004; Kumar and Clark, 2006). LC-MS/MS analysis of CYP metabolites remains the gold standard in industry but the throughput is limited by the number of samples that can be run in parallel and the analysis time of an individual sample. High-throughput fluorescent-based assays do exist; however, these assays are often an indirect measure of CYP activity, with inhibition of fluorescence in the presence of a fluorogenic substrate and a candidate substrate interpreted as an indication of activity (Trubetskoy et al., 2005). A recently developed high-throughput assay measures CYP activity indirectly by measuring oxygen and NADPH consumption via fluorescence but this assay requires multiple reagents and enzymes, and setting up the assay can be time-consuming (Traylor et al., 2011). In addition, laboratory or industrial use of CYPs is limited by the need for NADPH as the electron donor in the catalytic cycle. This is a major drawback of using CYPs for high-throughput screening or organic synthesis because NADPH is expensive, decomposes over time due to hydrolysis, and is difficult to recover once it has been oxidized (Udit and Gray, 2005).

Immobilizing CYPs on an electrode can obviate the need for NADPH and CPR as the electron donor and electron transfer partner enzymes, respectively, and the immobilized CYP can act as a biosensor by accepting electrons directly from the electrode (Bistolas et al., 2005). An increase in the current upon application of a potential can be correlated to catalytic activity of the enzyme against a candidate substrate. A CYP biosensor would be useful in the pharmaceutical industry as a tool for initial screens of drug candidates for reactivity with P450s and for potential drug–drug or food–drug interactions. A high-throughput electrode array, fabricated using techniques employed in semiconductor manufacturing, could even be used for personalized medicine by immobilizing CYP enzymes from an individual on the array and screening for CYP activity with different combinations of prescribed drugs.

Since the publication in the mid-1990 s of several studies on the electrochemistry of bacterial CYPs in solution or on bare electrodes (Estabrook et al., 1996; Reipa et al., 1997; Lo et al., 1999), there has been an explosion in the number of published CYP biosensor studies. Although initial studies on CYP biosensors were performed using adsorption on bare electrodes as the immobilization method, it has become apparent that the electrode environment greatly affects CYP electroactivity (Shumyantseva et al., 2005a). Modification of the electrode with protein-friendly materials prevents denaturation on the surface and has emerged as a better strategy for designing CYP biosensors. The types of electrode modifications used in CYP biosensor studies vary, as shown in Fig. 1 and Table 1, ranging from thin films with opposite charge adsorbed onto graphite to conductive polymers deposited onto noble metals such as gold or platinum. Most of these studies rely on a combination of electrochemical and analytical techniques to show that the CYP biosensor is electroactive and can detect different drug compounds via electrochemically-driven catalysis. However, a number of recent studies characterizing the active site structure and redox potential of CYPs immobilized on electrodes have shown that much of the CYP immobilized on the electrode is in an inactive form and call into question the results from previous CYP biosensor studies (Todorovic et al., 2006; Udit et al., 2006a; Bonifacio et al., 2008). In addition, some CYP biosensor studies are missing crucial substrate turnover data and instead rely on electrochemical experiments alone to indicate that the immobilized CYP is capable of electrochemically-driven catalysis (Sadeghi et al., 2011).

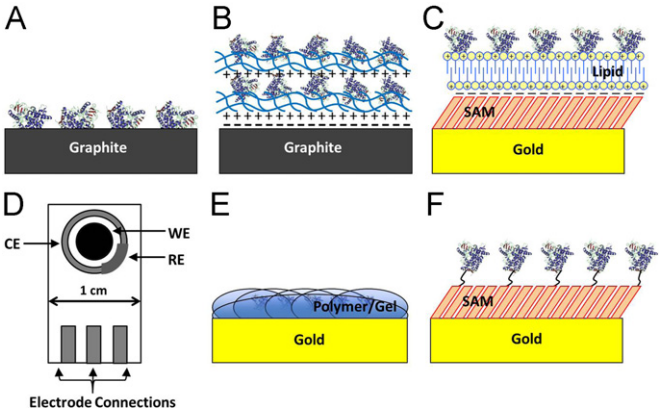

Fig. 1. Electrode immobilization strategies for the construction of CYP biosensors. (A) Adsorption to a bare electrode. (B) Layer-by-layer (LbL) adsorption. (C) Adsorption to a thin film. (D) Screen-printed electrode. (E) Encapsulation in polymers or gels. (F) Covalent attachment to self-assembled monolayers (SAMs) on a gold electrode.
Abbreviations: CE, counter electrode; WE, working electrode; RE, reference electrode.

This review focuses on the different electrode materials and immobilization strategies used to fabricate CYP biosensors, with special emphasis placed on characterization of the CYP electrode surface and electrochemically-mediated catalysis and detection of CYP substrates. An overview of electrode types and modifications is presented along with highlights of studies of particular interest. Primary attention will be given to biosensors based on the human drug-metabolizing CYPs; however, some studies based on bacterial CYPs are discussed because these studies served as a foundation for the development of mammalian CYP biosensors.

2. Electrode immobilization strategies

2.1. Adsorption to bare electrodes

Electrochemical investigations of the bacterial CYPs $P450_{CAM}$ (CYP101) and BM-3 (CYP102) on bare electrodes paved the way for current research on biosensors with drug-metabolizing CYPs. Initial studies employed a three-electrode electrochemical cell with bacterial CYPs in solution to reduce the enzyme and initiate substrate turnover. Fisher and co-workers used a mediator system with the soluble redox mediator cobalt(III) sepulchrate and a platinum wire working electrode to reduce BM-3 and other CYP fusion proteins, leading to a substrate turnover of 110 nmol/min/nmol P450 for the ω-hydroxylation of lauric acid by BM-3

Table 1
Summary of different electrode types and electrode modifications used to construct CYP electrodes and biosensors.

CYP enzyme	Electrode material	Electrode modification	Result	Reference
Adsorption to bare electrodes				
CYP101 ($P450_{CAM}$)	Edge-Plane Pyrolytic Graphite	None	Reversible peaks for Fe^{III}/Fe^{II} seen in anaerobic CV Increased reduction peak area in presence of D-(+)-camphor	Kazlauskaite et al., 1996
CYP101 Mutant SCF-K344C	Gold	None	Enhanced electroactivity of the SCF-K344C mutant	Lo et al., 1999
CYP2E1	Gold	None	Reversible peaks for Fe^{III}/Fe^{II} seen in anaerobic CV, $k_s = 5\ s^{-1}$	Fantuzzi et al., 2004
CYP199A2	Basal-Plane Pyrolytic Graphite	None	Quasi-reversible peaks for Fe^{III}/Fe^{II} seen in anaerobic CV, $k_s = 550$ s-1	Fleming et al., 2007
CYP101	Glassy Carbon	None	Increased reduction peak area in presence of D-(+)-camphor, $k_s = 0.016\ s^{-1}$	Mhaske et al., 2010
Layer-by-Layer Adsorption				
CYP101	Gold	Multilayer films of PSS and PDDA on an MPS SAM	Reversible peaks for Fe^{III}/Fe^{II} seen in anaerobic CV Electrochemically-driven styrene epoxidation (turnover $9.3\ h^{-1}$)	Lvov et al., 1998
CYP3A4	Gold	MPS SAM followed by PDDA	Reversible peaks for Fe^{III}/Fe^{II} seen in anaerobic CV Electrochemical detection of the 3A4 substrates verapamil and midazolam	Joseph et al., 2003
CYP1A2	Carbon Cloth	Alternate adsorption of PSS and 1A2	Reversible peaks for Fe^{III}/Fe^{II} seen in anaerobic CV Electrochemically-driven styrene epoxidation (turnover $39\ h^{-1}$)	Estavillo et al., 2003
CYP1A2 and CYP3A4 microsomes	Pyrolytic Graphite	Multilayer films of PEI and PSS	Reversible peaks for Fe^{III}/Fe^{II} seen in anaerobic CV Electrochemically-driven styrene epoxidation	Sultana et al., 2005
CYP1A2 and CYP2E1	Basal-Plane Pyrolytic Graphite	Multilayer films of CYP and CPR/b_5	Reversible reduction and oxidation peaks visible in anaerobic CV Evidence that electron transfer follows natural catalytic pathway from CPR Electrochemically-driven catalysis of NNK to HPB by 2E1 electrode	Krishnan et al., 2011
Adsorption to Thin Films				
CYP101	Glassy Carbon	Pretreated sodium montmorillonite clay colloid	Reversible peaks for Fe^{III}/Fe^{II} seen in anaerobic CV Fast electron transfer (5 to $152\ s^{-1}$ for scan rates of 0.4 to 12 V/s)	Lei et al., 2000
CYP2B4	Glassy Carbon	Mixture of sodium montmorillonite clay colloid, 2B4, and Tween 80	Reversible peaks for Fe^{III}/Fe^{II} seen in anaerobic CV Amperometric detection of the 2B4 substrates aminopyrine and benzphetamine	Shumyantseva et al., 2004
CYP101	Pyrolytic Graphite	DDAB or DMPC	Reversible peaks for Fe^{III}/Fe^{II} seen in anaerobic CV Relatively fast electron transfer with DDAB ($k_s = 26\ s^{-1}$) and DMPC ($k_s = 25\ s^{-1}$)	Zhang et al., 1997
CYP2C9, 2C18, and 2C19	Edge-Plane Pyrolytic Graphite	DDAB	Reversible peaks for Fe^{III}/Fe^{II} seen in anaerobic CV for all three enzymes Weak signal-to-background current and only 1–3% of enzyme is electroactive	Shukla et al., 2005
CYP2C9	Edge-Plane Pyrolytic Graphite	DDAB	Reversible peaks for Fe^{III}/Fe^{II} seen in anaerobic CV Anodic shift in redox potential with 2C9 substrates torsemide, warfarin, and tolbutamide and with CO	Johnson et al., 2005
CYP27B1	Edge-Plane Pyrolytic Graphite	DDAB	Reversible peaks for Fe^{III}/Fe^{II} seen in anaerobic CV ($k_s = 3.5\ s^{-1}$) No product formation observed during electrolysis with 27B1 substrate 25(OH)D_3	Rhieu et al., 2009
CYP3A4 fusion protein	Glassy Carbon	PDDA	Electrochemically-driven catalysis with the 3A4 substrate erythromycin	Dodhia et al., 2008
CYP101	Glassy Carbon	Covalent attachment to thin film of pyrene maleimide	Increased reduction peak area in the presence of D-(+)-camphor	Mhaske et al., 2010
Screen-Printed Electrodes				
Riboflavin-conjugated CYP1A2, 2B4, and 11A1	Rhodium-graphite	Mixture of CYP, BSA, glutaraldehyde, sodium cholate, and phospholipid	Electrochemically-driven catalysis with respective 1A2, 2B4, and 11A1 susbstrates Amperometric detection of the substrates aminopyrine (2B4) and cholesterol (11A1)	Shumyantseva et al., 2001
CYP1A2	Riboflavin-graphite	Glycerol and agarose	Amperometric detection of the 1A2 substrate clozapine	Antonini et al., 2003
CYP11A1	Rhodium-graphite	Gold nanoparticles	Amperometric detection of the 11A1 substrate cholesterol Enhanced electroactivity and sensitivity with inclusion of gold nanoparticles	Shumyantseva et al., 2005
CYP2B4	Carbon	Covalent attachment via EDC/NHS to a COOH-functionalized electrode	Amperometric detection of the 2B4 substrate cocaine in confiscated cocaine samples	Asturias-Arribas et al., 2011
CYP1A2, 2B4, and 51b1	Graphite	Mixture of gold nanoparticles and DDAB	Increased reduction peak area in the presence of substrates for 2B4 (benzphetamine) and 51b1	Shumyantseva et al., 2007

Table 1 (*continued*)

CYP enzyme	Electrode material	Electrode modification	Result	Reference
			(lanosterol) Enhanced electroactivity with inclusion of gold nanoparticles	
CYP2B4	Graphite	Mixture of gold nanoparticles and DDAB	Electrochemically-driven catalysis with benzphetamine exhibits similar uncoupling behavior to catalysis with 2B4 in solution	Rudakov et al., 2008
CYP2B4, 3A4, 11A1, 51b1	Graphite	Mixture of gold nanoparticles and DDAB	Amperometric detection of multiple substrates and inhibitors	Shumyantseva et al., 2011
Encapsulation in Polymers of Gels				
CYP101	Indium Tin Oxide	Polypyrrole	Electrochemically-driven catalysis with D-(+)-camphor	Sugihara et al., 1998
CYP102 ($P450_{BM-3}$) Mutant	Platinum and Glassy Carbon	Polypyrrole	Compared chemical vs. electrochemical polymerization of polypyrrole for effect on enzyme catalysis	Holtmann et al., 2009
CYP2B4	Gold	Polypyrrole	Amperometric detection of the 2B4 substrate phenobarbitol	Alonso-Lomillo et al., 2008
CYP101	Glassy Carbon	Methyltriethoxysilane sol-gel and DDAB	Reversible peaks for Fe^{III}/Fe^{II} seen in anaerobic CV in aqueous and organic media Amperometric detection of camphor and pyrene	Iwuoha et al., 2000
CYP2B6	Glassy Carbon	Mixture of chitosan and gold nanoparticles	Enhanced electroactivity with inclusion of chitosan and gold nanoparticles Electrochemically-driven catalysis of the 2B6 substrate bupropion	Liu et al., 2008
Covalent Attachment to Self-Assembled Monolayers on Gold				
CYP2C9	Gold	Amine coupling via EDC/NHS to a mixed SAM of OT and MUA	Quasi-reversible peaks for Fe^{III}/Fe^{II} seen in anaerobic CV Electrochemically-driven catalysis with the 2C9 substrate warfarin	Yang et al., 2009
CYP3A4 fusion protein	Gold	Amine coupling via EDC/NHS to a mixed SAM of 6HT and 7MHA	Microfluidic cell made of the 3A4 electrode amperometrically detected the 3A4 substrates quinidine, nifedipine, alosetron, and ondansetron	Fantuzzi et al., 2010
CYP2C9*1, 2C9*2, and 2C9*3 CYP2D6*1, 2D6*2, and 2D6*17	Gold	Amine coupling via EDC/NHS to a mixed SAM of 6HT and 7MHA (2C9) Maleimide/thiol coupling to maleimide-terminated SAM (2D6)	Micro-machined eight-electrode array used to amperometrically measure the K_M and k_{cat} values for the 2C9 substrate warfarin and the 2D6 substrate bufuralol	Panicco et al., 2011
CYPc17	Gold	His-tag attachment via modified Ni-NTA on an MPA SAM in the presence of DDAB	Redox peaks for Fe^{III}/Fe^{II} seen in anaerobic CV Enhanced electroactivity when using His-tag attachment vs. amine-coupling	Johnson and Martin, 2005
CYP2E1	Gold	Maleimide/thiol coupling to maleimide-terminated SAM	Redox peaks for Fe^{III}/Fe^{II} seen in anaerobic CV Faster ($k_s = 10\ s^{-1}$) electron transfer with maleimide/thiol coupling compared to adsorption to thin films	Fantuzzi et al., 2004
CYP2E1 Single-Cysteine Mutants	Gold	DTME SAM	Electrochemically-driven catalysis with the 2E1 substrate p-nitrophenol	Mak et al., 2010
CYP3A4 fusion protein	Gold	Maleimide/thiol coupling to maleimide-terminated SAM	Electrochemically-driven catalysis with the 3A4 substrate erythromycin	Dodhia et al., 2008
Future Directions/Nanostructured Electrodes				
CYP11A1	Rhodium-graphite	MWCNTs on screen-printed electrodes	Enhanced amperometric detection (improved linearity) of cholesterol with inclusion of MWCNTs	Carrara et al., 2008
CYP2B4, 2C9, 3A4	Graphite or Gold	MWCNTs on screen-printed electrodes	Amperometric detection of benzphetamine (2B4), naproxen (2C9), and cyclophosphamide Enhanced limits of detection with inclusion of MWCNTs	Cararra, et al., 2011
CYP3A4	Sputtered Gold	Adsorption to thin film of napthalene thiolate SAM	Enhanced electroactivity on sputtered gold electrodes ($k_s = 340\ s^{-1}$)	Mie et al., 2010
CYP3A4 microsomes	Microfabricated Gold Nanodomes	Adsorption to thin film of napthalene thiolate SAM	Enhanced electroactivity on nanostructured gold electrodes	Ikegami et al., 2011
CYP3A4	Gold	Amine coupling to ZnSe quantum dots covalently coupled to an MPA SAM	Amperometric detection of the 3A4 substrate 17β-estradiol Anodic shift in the redox potential with inclusion of quantum dots	Ndangili et al., 2011

(Estabrook et al., 1996). A similar study on the electrochemical reduction of $P450_{CAM}$ in solution used an antimony-doped tin oxide-coated working electrode with the natural electron transfer partner enzyme putidaredoxin (Pdr) as a mediator (Reipa et al., 1997). The authors were able to detect turnover of the $P450_{CAM}$ substrate camphor to the product 5-*exo*-camphor, and oxygen was supplied via water electrolysis at a platinum counter electrode. While neither of the abovementioned studies involved the physical immobilization of $P450_{CAM}$ and BM-3 on bare electrodes, the results from these indirect electrochemical systems validated that electrochemically-driven catalysis of CYPs was possible and sparked further research into the direct electrochemistry of CYPs and the construction of CYP biosensors.

Hill and co-workers observed the direct electrochemistry of $P450_{CAM}$ for the first time when it was adsorbed on a bare, edge-plane pyrolytic graphite (EPG) electrode (Kazlauskaite et al., 1996).

A follow-up study investigated the orientation of $P450_{CAM}$ on a bare gold electrode by creating a $P450_{CAM}$ mutant with one surface cysteine engineered on the proximal side (K344C) and the rest of the native surface cysteines mutated to alanines (Lo et al., 1999). Adsorption of this mutant (designated SCF-K344C) to a bare gold electrode resulted in enhanced electroactivity compared to both the WT enzyme and a surface cysteine-free mutant, as measured by the intensity of the cathodic peaks in the CVs. The results from this study suggest that the enhanced electroactivity of the SCF-K344C mutant may be due to a more effective orientation of the enzyme on the electrode surface. This is entirely plausible, as it is now known that a pocket of basic residues on the proximal sides of $P450_{CAM}$ and mammalian CYPs interacts with acidic residues on their respective electron transfer partner enzymes (Lewis and Hlavica, 2000; Hlavica et al., 2003).

It is well established that graphite electrodes such as glassy carbon (GC) and EPG are better able to promote the direct electrochemistry of CYPs than noble metal electrodes such as gold and platinum. Direct electrochemistry of the mammalian drug-metabolizing CYP2E1 was observed on a bare GC electrode in one of the first electrochemistry studies of a P450 enzyme from family 2 (Fantuzzi et al., 2004). Although a pair of reversible redox peaks was observed in CV scans with the GC/2E1 electrode, a higher electron transfer rate constant was determined with a modified gold electrode system ($k_s = 10\ s^{-1}$ versus $5\ s^{-1}$ for the bare GC electrode), suggesting that modification of the electrode surface enhances electron transfer. A more recent study of the cytochrome P450 enzyme CYP199A2 from the bacterium *Rhodopseudomonas palustris* adsorbed on a basal-plane pyrolytic graphite (BPG) electrode showed that the enzyme exhibited fast ($k_s = 550 \pm 50\ s^{-1}$) and quasi-reversible electron transfer with the electrode (Fleming et al., 2007). Another study on the direct electrochemistry of CYPs on graphite electrodes illustrates the advantages conferred by modification of the electrode. Mazumdar and co-workers covalently immobilized $P450_{CAM}$ to a GC electrode modified with pyrene maleimide by targeting native cysteine residues on the surface of the enzyme (Mhaske et al., 2010). Modifying the GC electrode with this conjugated ring system improved electron transfer between the electrode and $P450_{CAM}$, resulting in an electron transfer rate constant that was approximately 13 times greater than that of $P450_{CAM}$ adsorbed onto a bare GC electrode.

2.2. Layer-by-layer adsorption

One approach to modifying the electrode surface and providing a more protein-friendly environment for electrochemically-driven CYP catalysis is layer-by-layer (LbL) adsorption, a process by which multiple layers of oppositely-charged films and/or CYPs are built up on the electrode. In one of the first applications of the LbL technique, the Rusling group immobilized $P450_{CAM}$ on a gold electrode in multilayer films of either negatively charged poly(styrenesulfonate) (PSS) or positively charged poly(diallyldimethylammonium chloride) (PDDA) (Lvov et al., 1998). Multilayer films of $P450_{CAM}$/PDDA absorbed onto a gold electrode modified with a mercaptopropene sulfonic acid (MPS) SAM exhibited the highest turnover ($9.3\ h^{-1}$) of the substrate styrene, as indicated by the formation of styrene oxide during electrolysis with the Au-MPS-$(P450_{CAM}/PDDA)_2$ electrode. Using a similar LbL technique, Fuhr and co-workers made a CYP biosensor by immobilizing the human drug-metabolizing CYP 3A4 on a gold electrode modified sequentially with MPS and PDDA (Joseph et al., 2003). CV scans of the Au/MPS/PDDA/3A4 electrode showed reversible redox peaks with a midpoint potential of 98 ± 5 mV vs. NHE, and the biosensor was able to detect the 3A4 drug substrates verapamil and midazolam. In another study from the Rusling group, LbL adsorption was used to construct a CYP1A2 biosensor on carbon cloth (CC) electrodes by the alternate adsorption of PSS and 1A2 (Estavillo et al., 2003). The CC/PSS/$(CYP1A2/PSS)_2$ electrode exhibited nearly reversible electron transfer with a midpoint potential of -0.07 V vs. NHE and was able to catalyze the epoxidation of styrene at a turnover rate that was nearly 2.3 times that of 1A2-mediated epoxidation of styrene in solution with NADPH and CPR.

Several unique CYP biosensor configurations have been realized using the LbL adsorption technique. Sultana et al. immobilized CYP1A2 and 3A4 microsomes onto rough PG electrodes using an LbL assembly of polyethylenimine (PEI) and PSS films (Sultana et al., 2005). CV scans of the multilayer films $[CYP1A2ms/PEI]_6$ and $[CYP3A4ms/PEI]_6$ on PG electrodes gave reversible reduction and oxidation peaks at approximately -0.49 V vs. SCE, and the authors were able to detect electrochemically-driven styrene epoxidation. The difference between the redox potential of the microsome films and that of recombinant 1A2 or 3A4 in polyion films and the lack of a redox potential shift in the presence of carbon monoxide suggested that the electroactivity seen in the 1A2 and 3A4 microsome films was due to reduction of CPR and not P450. The discovery that microsomes are as effective as recombinant CYPs in promoting direct electrochemistry on electrodes is encouraging for the development of CYP biosensors because microsomes are cheaper to produce than recombinant CYPs and are already used in the pharmaceutical industry. A recent follow-up study of LbL films comprised of either recombinant CYP1A2 or 2E1 and CPR/cytochrome b_5-containing microsomes on BPG electrodes revealed that electron transfer in the CYP electrodes followed the natural catalytic pathway with electron transfer occurring first to CPR and then from CPR to the P450 (Krishnan et al., 2011). As seen in Fig. 2, 1A2 multilayers on BPG electrodes with CPR and b_5 exhibited reversible reduction and oxidation peaks in anaerobic CV scans and behaved nearly identically to digitally simulated CVs generated via a mathematical model of CYP electron transfer in vivo with CPR and b_5. In addition, a PDDA/PSS/$(CYP2E1/CPR+b_5)$ LbL film on a BPG electrode catalyzed the turnover of the substrate 4-(methylnitrosamino)-1-(3-pyridyl)-1-butanone (NNK) to 4-hydroxy-1-(3-pyridyl)-1-butanone (HPB) at a relative rate of 0.24 ± 0.04. Comparing this turnover rate to the turnover of NNK with 2E1 and NADPH/CPR in solution revealed that the multilayer 2E1 electrode was about 1.5 times more efficient at producing the HPB product.

2.3. Adsorption to thin films

There are numerous accounts in the literature of CYP biosensors constructed from thin films of lipid bilayers or polyelectrolytes absorbed onto electrodes. Deposition of thin films on the electrode surface is typically accomplished by simple drop-casting or a Langmuir trough. One of the first studies on CYPs adsorbed to thin film modified electrodes investigated the direct electrochemistry of $P450_{CAM}$ adsorbed to a GC electrode modified with a solution of the clay colloid sodium montmorillonite. The authors created a pretreated sodium montmorillonite colloid (PSMC) by mixing sodium montmorillonite colloid with colloidal Pt and created a GC/PSMC/$P450_{CAM}$ electrode via drop-casting (Lei et al., 2000). A similar study used a mixture of sodium montmorillonite colloid and the non-ionic detergent Tween 80 to immobilize the mammalian CYP 2B4 on a GC electrode (Shumyantseva et al., 2004). The authors detected reversible reduction and oxidation peaks for the GC/Clay+Tween/2B4 electrode at a formal potential of -295 mV vs. Ag/AgCl but were not able to detect any redox activity with a GC/Clay/2B4 electrode, underlining the

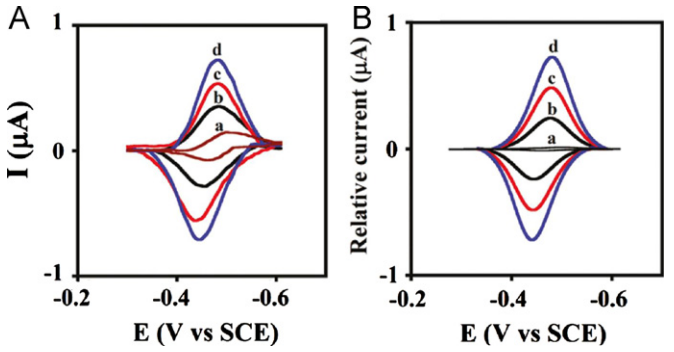

Fig. 2. Experimental and simulated CVs showing reversible electron transfer in a multilayer film of CYP1A2 and/or CPR/b_5 microsomes on a BPG electrode. (A) Experimental background-subtracted CVs of (a) PDDA/PSS-(/PDDA/CPR+b_5)$_6$ films with no CYP1A2 at 0.3 V/s and (b–d) PDDA/PSS-(/CYP1A2/CPR+b_5)$_6$ films at scan rates of (b) 0.1 V/s, (c) 0.2 V/s, and (d) 0.3 V/s. (B) Digitally simulated CVs of (a) electron transfer in PDDA/PSS-(/PDDA/CPR+b_5)$_6$ films with no CYP1A2 at 0.3 V/s and (b-d) electron transfer in PDDA/PSS-(/CYP1A2/CPR+b_5)$_6$ films at scan rates of (b) 0.1 V/s, (c), 0.2 V/s, and (d) 0.3 V/s assuming sequential electron transfer from reduced CPR to CYP1A2. Figure reproduced with permission from Krishnan et al., 2011.

importance of the nonionic detergent in promoting electron transfer. Although the GC/Clay+Tween/2B4 electrode had the highest electron transfer rate constant ($k_s > 114\ s^{-1}$), the highest amount of electroactive 2B4 was achieved when the sodium montmorillonite clay, Tween, and 2B4 were mixed together before deposition on the GC electrode, suggesting that surrounding the 2B4 with an ionic and lipophilic environment enhances its electroactivity. Using this immobilization strategy, the resulting 2B4 electrode was used to amperometrically detect the drug substrates aminopyrine and benzphetamine, and catalytic turnover of aminopyrine was confirmed by quantifying formaldehyde, the product of aminopyrine-N-demethylation. In a related study, Wang and co-workers used a composite film of nano sodium montmorillonite clay and the detergent dihexadecylphosphate to immobilize rat CYP1A1 on an EPG electrode (Wu et al., 2011). The CYP1A1 electrode exhibited a pair of redox peaks with a formal potential of -0.36 V vs. SCE and amperometrically detected the compound benzo[*a*]pyrene. The results from these studies suggest that thin films of clay nanoparticles can be used to fabricate efficient CYP biosensors.

Thin films of lipid bilayers are especially attractive because they are thought to recapitulate the lipophilic environment of the smooth endoplasmic reticulum where most mammalian CYPs reside. The majority of CYP biosensor studies utilizing thin films of lipid bilayers on electrodes use the cationic lipid didodecyldimethylammonium bromide (DDAB) on GC or EPG electrodes, although phospholipids such as L-α-phosphatidylcholine dimyristoyl (DMPC) have also been used (Zhang et al., 1997; Fleming et al., 2006). DDAB forms a stable lipid bilayer at room temperature and the positive charge on the ammonium ion allows it to interact electrostatically with negatively charged graphite electrodes. The Rusling group pioneered the use of biomembrane-like films in CYP biosensors by using thin films of DDAB or DMPC to create electrochemically active $P450_{CAM}$ on PG electrodes (Zhang et al., 1997). Numerous research groups have used the same approach to create electrochemically active mammalian CYPs. Bernhardt and co-workers reported the direct electrochemistry of P450s from the 2C family for the first time using thin films of DDAB on EPG electrodes (Shukla et al., 2005). The human drug-metabolizing CYPs 2C9, 2C18, and 2C19 were immobilized separately on EPG electrodes by drop-casting a mixture of CYP and an aqueous dispersion of DDAB on EPG. For all three enzymes, a single Fe^{III}/Fe^{II} redox potential was identified but the signal-to-background current was very weak and only a small (1–3%) amount of the total immobilized enzyme was electroactive. A similar study published at the same time characterized the direct electrochemistry of CYP2C9 adsorbed on a DDAB-modified EPG electrode (Johnson et al., 2005). A pair of redox peaks centered at −41 mV vs. Ag/AgCl was seen for the GC/DDAB/2C9 electrode, and this redox process was found to be surface-confined based on the linear relationship between the peak anodic and cathodic currents and the scan rate. Although it was not determined whether the 2C9 electrode was capable of substrate turnover, an anodic shift in the redox potential in the presence of CO and the 2C9 substrates torsemide, tolbutamide, and warfarin suggested that the immobilized 2C9 was in a conformation that allowed for substrate binding. The authors noted that the measured redox potential of −41 mV for the GC/DDAB/2C9 electrode was much higher than the reported redox potentials in solution. This is the case for most CYP electrodes and is purported to be a result of conformation changes or dehydration induced upon immobilization. A recent study has extended the use of DDAB films on electrodes to the mitochondrial CYP27B1, which catalyzes the hydroxylation of 25-hydroxyvitamin D_3 ($25(OH)D_3$) to its active metabolite. Recombinant mouse CYP27B1 was adsorbed onto EPG disc electrodes modified with DDAB, and the EPG/DDAB/27B1 electrode exhibited nearly symmetric redox peaks with a midpoint potential of −180 mV vs. Ag/AgCl (Rhieu et al., 2009). Interestingly, no product formation was observed during electrolysis of the 27B1 electrode in the presence of $25(OH)D_3$; the authors proposed that DDAB may be blocking the enzyme's active site, a phenomenon that has been documented before with the surfactant SDS (Udit et al., 2006b).

2.4. Screen-printed electrodes

Screen-printed electrodes are ideal for constructing CYP biosensors because screen-printing is inexpensive and a number of conductive additives such as rhodium graphite or gold nanoparticles can be mixed directly into the electrode paste. In addition, electrodes of many different sizes and configurations can be made using screen-printing, making the construction of a CYP biosensor array relatively simple. The Shumyantseva group has been studying the direct electrochemistry of CYPs on screen-printed electrodes for more than a decade, in particular the direct electrochemistry of CYP11A1 (P450scc), the CYP responsible for the side chain cleavage reaction of cholesterol. One of their first studies involved the immobilization of the riboflavin-P450 conjugates RfP4501A2, RfP4502B4, and RfP450scc on rhodium graphite screen-printed thick film electrodes (Shumyantseva et al., 2001). The Rf-P450 conjugates were immobilized onto screen-printed electrodes by drop-casting a solution of the Rf-P450, BSA, glutaraldehyde, sodium cholate, and phospholipid onto the electrode surface, and all three Rf-P450 electrodes were capable of electrochemically-driven turnover with their respective substrates. Amperometric responses were observed with the RfP4502B4 and RfP450scc electrodes in the presence of aminopyrine and cholesterol, respectively, showing that the CYP electrodes acted as biosensors. A related study used riboflavin–graphite screen-printed electrodes to construct a CYP1A2 biosensor. The 1A2 was immobilized on a screen-printed electrode by encapsulation in a glycerol and agarose gel matrix, and the resulting 1A2 electrode was able to electrochemically detect increasing concentrations of the drug clozapine (Antonini et al., 2003).

Gold nanoparticles (AuNP) were used to enhance the electroactivity of P450scc on rhodium–graphite screen-printed electrodes in another study by the Shumyantseva group (Shumyantseva et al., (2005b)). The reduction current of the P450scc electrode

was significantly enhanced in the presence of the gold nanoparticles, and the authors suggested that the rough electrode surface imparted by the nanoparticles provided for more intimate electrical contact with the enzyme. Interestingly, the AuNP-P450scc electrode was more sensitive in detecting cholesterol than the aforementioned RfP450scc electrode, further suggesting that the gold nanoparticles enhanced the electroactivity of P450scc. The human drug-metabolizing CYP 2B4 was covalently immobilized on a screen-printed carbon electrode for the detection of cocaine in a recent study by Arcos-Martínez and co-workers (Asturias-Arribas et al., 2011). The 2B4 was amine-coupled to a screen-printed carbon electrode functionalized with carboxylic acid groups, and the resulting 2B4 biosensor accurately determined the concentration of cocaine in confiscated street cocaine samples and had a limit of detection (LOD) of 23.05 ± 3.53 nM.

Screen-printed electrodes have also been used in conjunction with the lipid DDAB to construct CYP biosensors. CYP2B4, 1A2, and 51b1 (sterol-14α-demethylase) were prepared on screen-printed graphite electrodes modified with a mixture of gold nanoparticles and DDAB (Shumyantseva et al., 2007). Aerobic CV scans of the DDAB/AuNP/2B4 and DDAB/Au-NP/51b1 electrodes showed midpoint potentials of -393 and -437 mV vs. Ag/AgCl, respectively, and the electrodes were sensitive to their respective substrates benzphetamine and lanosterol. A comparison between the DDAB/AuNP/2B4 and DDAB/2B4 electrodes revealed that the gold nanoparticles enhanced the observed reduction current in aerobic CV scans. In an interesting follow-up study, the same research group investigated the stoichiometry of electrochemically-driven benzphetamine catalysis with a DDAB/AuNP/2B4 electrode (Rudakov et al., 2008). The authors tracked the formation of H_2O_2, consumption of O_2, and formation of the product formaldehyde over time to investigate the extent of uncoupling that occurs during electrolysis with the 2B4 electrode. Uncoupling occurs when reduction of the P450 heme does not lead to product formation and instead results in the unproductive release of reactive oxygen species that short-cut the natural catalytic cycle. A bi-electrode scheme with a Prussian blue (PB) electrode and Clark oxygen electrode was used to electrochemically measure the formation of H_2O_2 and the consumption of O_2, respectively, with time. The results, seen in Table 2, showed that although the electrochemical reduction of 2B4 does lead to uncoupling and the formation of H_2O_2, the electrochemically-derived rates for H_2O_2 production, O_2 consumption, and product (formaldehyde) formation are similar to those found in the microsomal system with NADPH. This suggests that, at least for the DDAB/AuNP/2B4 system, catalysis on an electrode is a comparable substitute to NADPH-mediated catalysis and can be used to study the electrochemistry of CYPs in vitro. This DDAB/AuNP system was extended to other CYPs and multiple substrates in a recent study, where CYP3A4 and 11A1 (P450ssc), in addition to 2B4 and 51bl, were immobilized on screen-printed graphite electrodes modified with DDAB and gold nanoparticles (Shumyantseva et al., 2011). Multiple substrates and inhibitors were detected with the different CYP electrodes, implying that this novel DDAB/AuNP system could be a universal method for the construction of a screen-printed array of CYP biosensors.

2.5. Encapsulation in polymers or gels

Several CYP biosensor studies have used encapsulation in polymers or gels to immobilize P450s on an electrode and enhance their electroactivity. The majority of these studies use the conductive polymer polypyrrole to entrap the P450 on an electrode and enmesh it in a conductive matrix; however, other conductive polymers such as polyacetylene have also been used. $P450_{CAM}$ was immobilized in polypyrrole polymerized on an indium tin oxide (ITO) electrode in one of the first published examples of a CYP biosensor prepared via the encapsulation technique (Sugihara et al., 1998). Polypyrrole was electropolymerized on the surface of the ITO electrode in the presence of various concentrations of $P450_{CAM}$, and the resulting $P450_{CAM}$ electrode was capable of electrochemically-driven catalysis as evidenced by the presence of hydroxycamphor in the electrolyte after controlled potential electrolysis with the substrate camphor. In a similar study, a quintuple P450 BM-3 mutant was immobilized in polypyrrole on Pt wire and GC electrodes, and both types of electrodes were capable of substrate turnover with the model substrate *p*-nitrophenoxycarboxylic acid (p-NCA) (Holtmann et al., 2009). The authors compared two different polypyrrole polymerization procedures (chemical vs. electrochemical) for their effect on BM-3 activity and concluded that electropolymerization had less of an effect on enzyme activity. In a more recent study, a CYP2B4 biosensor was constructed using a miniaturized three electrode chip fabricated by photolithography, and the 2B4 was immobilized on a gold working electrode via encapsulation in polypyrrole (Alonso-Lomillo et al., 2008). Chronoamperograms of the 2B4 electrode polarized at 0.45 V vs. Ag/AgCl showed a current response proportional to the concentration of the substrate phenobarbital, and the 2B4 biosensor accurately determined the concentration of phenobarbital (4.049 mM) in a commercial pharmaceutical. In a study published this year, a CYP3A4 biosensor was successfully created by immobilizing 3A4 in a conductive epoxy film on a GC electrode (Dai et al., 2012). The conductive epoxy film consisted of a mixture of epoxy copolymers and polyacetylene, and the 3A4 biosensor responded amperometrically to increasing concentrations of diethylstilbestrol.

Table 2
Electrochemically-derived and microsomally-derived rates of H_2O_2 production, O_2 consumption, and product (formaldehyde) formation by CYP2B4. Electrochemically-derived rates were measured using a DDAB/AuNP/2B4 graphite screen-printed electrode at a controlled potential of -0.450 V vs. Ag/AgCl for 1 h in 0.1 M KPi, pH 7.4, containing 0.05 M NaCl, and 0.5 mM benzphetamine was used as substrate. [a]Values are calculated per electroactive enzyme. [b]Data taken from Zhukov and Archakov, 1985. Table values reproduced with permission from Rudakov et al., 2008.

	H_2O_2 Produced (nmol/nmol of enzyme/min)			O_2 Consumption (nmol/nmol of enzyme/min)	Product (formaldehyde) Formation Rate (nmol/nmol of enzyme/min)
	Spectrophotometry	Amperometry		Amperometry	Spectrophotometry
	Horseradish peroxidase/ABTS	PB-Electrode	Cyt *c* Electrode	Clark Electrode	Nash Reagent
Absence of substrate ($E^{0'} = -0.450$ V)	4.3 ± 0.7	4.4 ± 0.7	5.6 ± 0.8	4.8 ± 0.4	–
Presence of substrate ($E^{0'} = -0.450$ V)	2.6 ± 0.5	3.0 ± 0.5	4.3 ± 0.7	19.4 ± 0.6	17 ± 3[b]
Microsomes[a] free oxidation NADPH	3.14	–	–	3.6 ± 0.2	–
Microsomes[b] benzphetamine NADPH	2.8	–	–	21.6 ± 0.6	14.4 ± 0.5

Hydrophilic gels such as agarose, chitosan, and sol–gels have also been used to encapsulate CYPs on electrodes and facilitate electron transfer. Additives such as nanoparticles or lipids have been added to gels to enhance the conductivity and/or stability of the immobilized CYP. Iwuoha et al. used a methyltriethoxysilane (MTEOS) sol–gel to encapsulate $P450_{CAM}$ on a GC electrode (Iwuoha et al., 2000). DDAB was added to the $P450_{CAM}$ prior to encapsulation, resulting in a biomembrane-like environment on the surface of the electrode. CV scans of the resulting GCE-[$P450_{CAM}$/DDAB/SG] electrode in phosphate buffer and in 90% acetonitrile revealed a pair of redox peaks, and the $P450_{CAM}$ biosensor was capable of detecting 3 mM of the substrate camphor or pyrene in aerobic phosphate buffer. Surprisingly, the authors noted that the biosensor exhibited faster reversible electron transfer in 90% acetonitrile than in water and attributed this to the increased fluidity of DDAB in acetonitrile and relaxation of the sol–gel/enzyme layer. Sol–gel encapsulation also maintained the activity of the immobilized $P450_{CAM}$ for up to four weeks. The natural polysaccharide chitosan mixed with gold nanoparticles was used to encapsulate the human drug-metabolizing enzyme CYP 2B6 on a GC electrode; the resulting 2B6 electrode was used as a biosensor to amperometrically detect the drugs lidocaine, cyclophosphamide, and bupropion (Liu et al., 2008). The gold nanoparticles were prepared in a chitosan solution and mixed with the P450 prior to drop-casting on the surface of the GC electrode. The authors observed enhanced peak currents for the GC/AuNP-chitosan/2B6 electrode when compared to a GC/2B6 electrode, suggesting that the gold nanoparticles and chitosan film facilitated facile electron transfer to the P450. Absorption spectra of a glass slide coated with an AuNP-chitosan/2B6 film revealed that the absorption band for colloidal gold was red-shifted from 536 to 541 nm, indicating an interaction between the enzyme and gold nanoparticles. Electrospray ionization mass spectrometry (ESI-MS) detected the catalytic product hydroxybupropion after controlled potential electrolysis, confirming that the 2B6 electrode was capable of substrate turnover.

2.6. Covalent attachment to self-assembled monolayers on gold

Covalent attachment of CYPs to gold electrodes via SAMs has proven to be a robust and simple technique for creating CYP biosensors. Long or short chain n-alkanethiols form an ordered monolayer, or SAM, on gold due to the high affinity of sulfhydryl groups (–SH) for gold and favorable van der Waals interactions between alkane chains. SAMs with various termini can be used to modify gold electrodes with functional groups such as carboxyls, amines, and maleimides to facilitate different immobilization chemistries. No clear consensus exists in the CYP biosensor literature on whether short or long chain SAMs are better at promoting electron transfer but it is well known that short chain SAMs create a diffuse and less ordered monolayer whereas long chain SAMs create a densely packed and well-ordered monolayer. Many CYP biosensor studies with SAMs use long chain alkanethiols such as 11-mercaptoundecanoic acid (MUA) or hexanoic acid but there are also examples of using shorter chain thiols such as dithio-bismaleimidoethane (DTME) to immobilize CYPs (Mak et al., 2010). Long chain SAMs may help stabilize the immobilized CYP and prevent surface denaturation; however, there is a trade-off in electroactivity when using long chain SAMs because the electron transfer rate constant decreases exponentially with the chain length, *n*, of the SAM (Nikki and Gregory, 2003). A recent study illustrated this phenomenon quite well; Zhang and co-workers compared the surface coverage and electron transfer resistance of MUA and MPA SAMs on gold nanopillar modified electrodes using CV and electrochemical impedance spectroscopy (EIS) (Anandan et al., 2009). The MUA SAM had the higher surface coverage of 62.2% but its electron transfer resistance (209 kΩ) was approximately 33-times that of the MPA SAM, and a glucose oxidase (GOx) biosensor made from the MPA coated electrode was six-times more sensitive at detecting glucose than one made with an MUA coated electrode.

Several different immobilization chemistries have been used to covalently attach CYPs to SAMs formed on gold electrodes. The most common immobilization chemistry is amine coupling and uses the reagents EDC (1-Ethyl-3-[3-dimethylaminopropyl] carbodiimide hydrochloride) and NHS (N-hydroxysuccinimide) to attach the P450 to a carboxy-terminated SAM on gold via surface exposed amine groups (lysine residues). Although this attachment chemistry is fairly simple and widely used, the immobilized CYP is tethered to the electrode in a random orientation based on the number and reactivity of surface exposed amines. Nevertheless, different research groups have covalently coupled CYPs to carboxy SAMs on gold via amine coupling and observed electroactivity even though the immobilized CYP may not be oriented optimally for electron transfer. CYP2C9 was immobilized to a gold electrode via amine coupling to a mixed SAM of 3:1 octanethiol (OT) and MUA. An anaerobic CV scan of the Au/OT-MUA/2C9 electrode revealed quasi-reversible reduction and oxidation peaks at a formal potential of −0.49 and −0.42 V vs. Ag/AgCl, respectively, and detection of the metabolite 7-hydroxywarfarin in the electrolyte after controlled potential electrolysis with the 2C9 substrate warfarin confirmed that the 2C9 biosensor was capable of electrochemically-driven catalysis (Yang et al., 2009). More recently, Fantuzzi et al. used amine coupling to a mixed SAM of 1:1 6-hexanethiol (6HT) and 7-mercaptoheptanoic acid (7MHA) to immobilize a fusion protein of CYP3A4 and flavodoxin (FLD) to gold electrodes prepared via photolithography (Fantuzzi et al., 2010). Fusing 3A4 with the flavodoxin from *Desulfovibrio vulgaris* was shown earlier by the same research group to improve the coupling efficiency of 3A4 on gold and GC electrodes (Dodhia et al., 2008). A microfluidic cell (Fig. 3) consisting of the Au/6HT-7MHA/3A4-FLD electrode, a screen-printed carbon counter electrode, and a screen-printed Ag/AgCl reference electrode was used to detect the 3A4 substrates quinidine, nifedipine, alosetron, and ondansetron, and the K_M values for these substrates were determined. Although there was some variability between the microfluidically-measured K_M values and K_M values in the literature, the relative ranking of the substrates from low to high K_M matched that reported in the literature, suggesting that the 3A4-FLD biosensor could be used as an initial screen for 3A4 reactivity of test compounds. A follow-up study employed the same immobilization strategy with 6HT and 7MHA SAMs to attach polymorphic variants of CYP2C9 to gold electrodes in an eight-electrode array (Panicco et al., 2011). As in the aforementioned studies with 3A4, the variants 2C9*1 (wild-type), 2C9*2 (R144C), and 2C9*3 (I359L) were fused separately to the flavodoxin from *D. vulgaris*. A commercially available strip of micromachined electrodes in 300-μL wells formed an eight-electrode array, and the 2C9 biosensors were used to measure the K_M and k_{cat} values of the substrate warfarin with the different 2C9 variants. Although the amperometrically-determined K_M values were notably smaller than those in the literature, a relative ranking of the 2C9 variants based on electrochemically-driven formation of the product hydroxywarfarin again matched the published trend.

Oriented attachment of CYPs to SAMs on gold electrodes has been achieved via site-specific attachment at certain residues such as cysteines. Johnson and Martin oriented his-tagged bovine P450c17 at the C-terminus on a gold electrode by modifying an MPA SAM on gold with nickel-charged Acbztacn (1-acetato-4-benzyl-triazacyclononane), an alternative to Ni-NTA (Johnson and Martin, 2005). Surface plasmon resonance experiments revealed

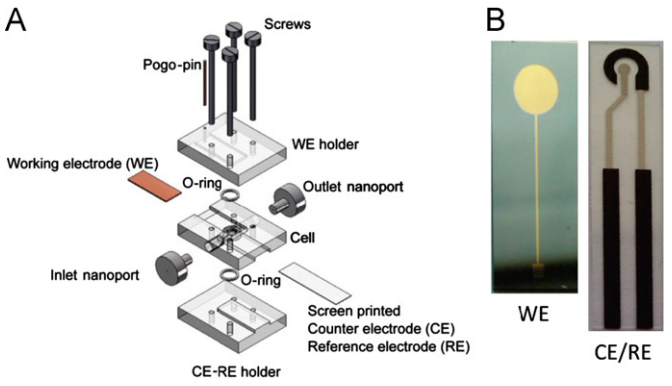

Fig. 3. Microfluidic cell used to detect the 3A4 substrates quinidine, nifedipine, alosetron, and ondansetron. (A) Schematic of the poly (methylmethacrylate) microfluidic cell consisting of a flow cell, working electrode, and screen-printed counter and reference electrodes. (B) Enlarged view of the evaporated gold working electrode (WE), screen-printed carbon counter electrode (CE), and screen-printed Ag/AgCl reference electrode (RE). Figure reproduced with permission from Fantuzzi et al., 2010.

that the Ni-Acbztacn surface did not experience any metal leaching over a 24 hour period, and the presence of redox peaks in an anaerobic CV scan of the Au/Ni-Acbztacn/P450c17 electrode in the presence of DDAB showed that the immobilized P450c17 was electroactive. SAMs modified with maleimide groups have been used to site-specifically attach CYPs to electrodes at cysteine residues (thiols). One of the first examples of this immobilization strategy was the covalent attachment of CYP2E1 to a gold electrode (Fantuzzi et al., 2004). A gold electrode was modified sequentially with a cystamine SAM (CYSAM) and an amine-reactive maleimide, and recombinant 2E1 was incubated overnight on the maleimide-functionalized electrode to create a 2E1 biosensor. The authors compared the Au/CYSAM/MALIM/2E1 electrode to 2E1 electrodes fashioned from bare GC, GC/DDAB, GC/PDDA, and Au/MPA/PDDA electrodes and found that the maleimide modified electrode exhibited the highest electron transfer rate constant ($10 \pm 0.5\ s^{-1}$). Analysis of the crystal structure of 2E1 revealed the presence of two surface cysteines, C261 and C268, on the proximal face of the enzyme with surface exposures of 37 and 25%, respectively, and the authors suggested that attachment at these residues may have resulted in oriented attachment of 2E1 on the proximal side and enhanced electron transfer to the heme. A related study by the same research group characterized the electrocatalytic response of recombinant 2E1 mutants attached specifically at C261 or C268 to gold electrodes modified with a DTME SAM (Mak et al., 2010). MUT261 and MUT268 were created by mutating all the surface cysteine residues to serines save for C261 and C268, respectively. After 30 min of electrolysis in the presence of the 2E1 substrate *p*-nitrophenol, the amount of product *p*-nitrocatechol in the electrolyte was determined spectrophotometrically for the different 2E1 electrodes. The MUT261 and MUT268 electrodes produced, respectively, 2.6- and 2.1-times as much *p*-nitrocatechol as the wild-type 2E1 electrode, suggesting that orienting the enzyme on the electrode enhanced its electroactivity.

A maleimide-functionalized SAM was also used to immobilize the CYP2D6 polymorphic variants 2D6*1 (wild-type), 2D6*2, and 2D6*17 on a gold electrode (Panicco et al., 2011). An eight-electrode array of gold electrodes was modified sequentially with a 6-aminohexanethiol SAM and N-succinimidyl-3-maleimidopropionate to create maleimide functionalized electrodes. N-succinimidyl-3-maleimidopropionate was identified in an earlier study by the same research group as being superior to DTME for functionalization of gold electrodes with maleimide groups and therefore was used in place of DTME (Ferroro et al., 2008). The resulting 2D6 biosensors were used to measure the K_M and k_{cat} values of the different 2D6 variants with the substrate bufuralol, and the polymorphic variants were distinguishable from one another by their different K_M and k_{cat} values, which were in good agreement with results from the literature. However, unlike the aforementioned studies with 2E1, the authors did not comment on which residues on 2D6 most likely reacted with the maleimide surface and whether the 2D6 variants were attached to the electrode surface in a defined orientation.

3. Characterization of CYP electrodes

The majority of CYP biosensor studies use electrochemical techniques such as cyclic voltammetry or chronoamperometry to show that the immobilized CYP is electroactive and capable of substrate turnover. However, little information exists on the conformation of CYPs immobilized on electrodes and the effect, if any, that structural changes induced by immobilization have on catalysis. There is some evidence to suggest that CYPs undergo a conformational change upon electrode immobilization that results in the formation of P420, an inactive CYP species characterized by absorption of the reduced ferrous heme at 420 nm. Formation of P420 is believed to occur via structural changes in the enzyme that result in protonation of the axial thiolate ligand and perturbation of the electronic environment of the heme (Perera et al., 2003). Formation of P420 has been induced by increases in temperature (Mouro et al., 1997) and/or pressure (Hui Bon Hoa et al., 1989) and exposure to neutral salts (Imai and Sato, 1967), detergents (Omura and Sato, 1964), organic solvents (Yu and Gunsalus, 1974), and high/low pH buffers (O'Keefe et al., 1978). In a study by Hill and co-workers, immobilization of the bacterial P450 BM-3 in thin films of the surfactant DDAB was found to induce formation of the inactive P420 species over time (Udit et al., 2006a). A difference spectrum of the reduced (Fe^{II}) BM-3 bound to CO revealed the presence of a 420 nm peak after a two-minute incubation in a DDAB dispersion. A CV scan at 25 mV/s of a BPG/DDAB/BM-3 electrode showed well-defined, reversible redox peaks centered at -260 mV vs. SCE, suggesting that even though some of the enzyme was in the inactive P420 form electron transfer to and from the iron heme was still possible. The authors noted that the BM-3 Fe^{III}/Fe^{II} redox potential in DDAB was approximately 300 mV more positive than the redox potential in solution and attributed this anodic potential shift to stabilization of the ferrous (Fe^{II}) heme in the P420 state. In a similar study, Gilardi and co-workers investigated the effects of the polycations PEI and PDDA on the absorption spectra of the heme domain of P450 BM-3 (BMP) immobilized on mesoporous tin-oxide (SnO_2) electrodes (Panicco et al., 2008). Using cyclic voltabsorptometry, the authors were able to measure the absorption spectra of immobilized BM-3 during cyclic voltammetry. Electrochemical reduction of the SnO_2/PEI/BMP electrode in the presence of CO resulted in the formation of the inactive P420 species while no P420 was detected during reduction of the SnO_2/PDDA/BMP electrode. PDDA seemed to inhibit formation of the inactive P420 form and stabilize the Fe^{II}–CO complex in an active conformation. This result is in stark contrast to the finding that DDAB induces formation of P420 upon immobilization of BM-3 on an electrode, and the fact that both PEI and DDAB have been used in CYP biosensor studies calls into question whether the electrochemical responses exhibited by these sensors were actually from inactive P420 instead of active CYP.

Formation of the inactive P420 species has also been observed for bacterial and mammalian CYPs immobilized to SAMs on electrodes. Surface-enhanced resonance Raman spectroscopy (SERRS) of $P450_{CAM}$ adsorbed to an MUA SAM on a silver (Ag)

electrode revealed that both the ferric and ferrous states of the enzyme were predominantly in the P420 form (Todorovic et al., 2006). The authors attempted to mitigate the formation of P420 by increasing the ionic strength, introducing methyl-terminated alkanethiols into the SAM, decreasing the pH, or by coupling the CYP to the carboxylate SAM via amines. None of these methods resulted in stabilization of the native P450 state, suggesting that conformational changes induced by the high electric field inherent on the surface of the electrode were solely responsible for the formation of inactive P420. Increasing the number of methylene units, *n*, of the carboxylate SAM on Ag resulted in a positive shift in the redox potential of the immobilized CYP, most likely due to a stabilizing effect of the longer chain SAMs on the ferrous form of the enzyme. Shortening the length of the ω-carboxylate SAM had the opposite effect: the redox potential exhibited a negative shift. In this case, the authors proposed that the high electric field closer to the electrode surface stabilizes the positively charged ferric form of the enzyme, resulting in a more negative redox potential.

A similar study used SERRS to investigate the active site structure, substrate binding, and redox activity of the drug-metabolizing CYP 2D6 adsorbed to an MUA SAM on a silver electrode (Bonifacio et al., 2008). SERRS spectra revealed that the enzyme retained its native structure upon immobilization and was able to reversibly bind the substrate dextromethorphan. Electrochemical reduction of the 2D6 enzyme, however, was not possible, and SERRS spectra taken of the Ag/MUA/2D6 electrode polarized at negative potentials contained marker bands at 1371 and 1360 cm^{-1} for the ferric and P420 forms of the enzyme, respectively. Based on these results, the authors concluded that electrodes coated with an MUA SAM were not suitable for the direct electrochemistry of 2D6. This is an interesting result, considering that MUA coated gold electrodes promoted the direct electrochemistry and electrochemically-driven catalysis of CYP2C9 in a previous study (Yang et al., 2009).

Atomic force microscopy (AFM) and scanning tunneling microscopy (STM) can also be used to characterize the surface of CYP electrodes but few CYP biosensor studies in the literature have taken advantage of these techniques. AFM can be used to assess the orientation of an enzyme on the electrode surface, while STM with electrochemical control (EC-STM) is especially useful as it allows for imaging of the electrode surface at different applied potentials. As shown in Fig. 4, an EC-STM image of a cysteine mutant of the electroactive metalloprotein poplar plastocyanin (PCSS) adsorbed on gold taken at a potential near its redox potential (106 mV vs. SCE) exhibits markedly higher contrast than an image taken at a potential far from the redox potential (Bonanni et al., 2007). Thus, the contrast of EC-STM images taken under different potentials can be used to estimate the electroactivity and redox potential of an electrode-immobilized CYP (Tao, 1996).

A study by Davis et al. used STM to probe the orientation of a $P450_{CAM}$ mutant (SCF-K344C) adsorbed to a gold electrode (Davis et al., 2000). The authors mutated all the surface-exposed cysteines on $P450_{CAM}$ to chemically inert alanines and mutated one lysine residue (K344) on the proximal side of the enzyme closest to the heme to a cysteine. STM images of the SCF-K344C mutant on gold revealed an ordered and compact monolayer of enzyme on the surface whereas images of the wild-type enzyme showed a random and unstructured monolayer, suggesting that the specific cysteine mutation of the SCF-K344C mutant oriented the enzyme on the surface of the electrode. Gilardi and co-workers used a similar approach to immobilize a CYP2E1 fusion protein on a maleimide-functionalized SAM attached to gold, and the authors used tapping-mode AFM (TMAFM) to image a monolayer of 2E1 on the electrode (Sadeghi et al., 2011). The same research group also used TMAFM to image single-cysteine mutants of the BM-3 heme domain BMP immobilized on gold electrodes via a maleimide-functionalized SAM (Ferroro et al., 2008). Two surface cysteines, C156 and C62, were mutated individually to serines such that attachment to a maleimide gold electrode occurred at only one surface cysteine residue. As shown in Fig. 5, TMAFM images of wild-type BMP, C156S, and C62S immobilized on the maleimide-coated gold electrode showed that immobilization of the C156S mutant at residue C62 resulted in a stable and well-ordered monolayer. An analysis of the crystal structure of BMP revealed that residues C62 and C156 had a solvent accessibility of 11.6 and 1.0 $Å^2$, respectively. The authors proposed that the increased solvent accessibility of residue C62 allowed for enhanced binding of the C156S mutant to maleimide-functionalized gold and the formation of an ordered enzyme monolayer.

4. Recent innovations

CYP biosensors are increasingly being made with microfabricated electrodes or nanostructured materials such as multi-walled carbon nanotubes (MWCNTs). Microfabricated CYP biosensors and array-based systems integrated with microfluidics are bringing portable CYP biosensors closer to reality while nanostructured electrodes increase the active surface area for electron transfer and allow for more intimate contact with the immobilized CYP. Combining nanostructured materials with microfabricated electrode arrays, one can imagine the creation of a portable CYP biosensor chip for use at a doctor's office or patient's bedside for personalized medicine. MWCNTs were used by Carrara et al. to promote the direct electrochemistry of P450scc on rhodium-graphite screen-printed electrodes (Carrara et al., 2008). The MWCNTs were deposited on the rhodium-graphite electrodes by drop-casting, and aerobic CV scans of the MWCNT-modified P450scc electrode showed a marked increase in the cathodic current when compared to a P450scc electrode modified with gold nanoparticles. The MWCNT-modified P450scc electrode functioned as a biosensor for the amperometric detection of cholesterol; its sensitivity of 1.12 $\mu A/(mM \cdot mm^2)$ was similar to that of a P450scc biosensor made with gold nanoparticles but the carbon nanotubes considerably improved the

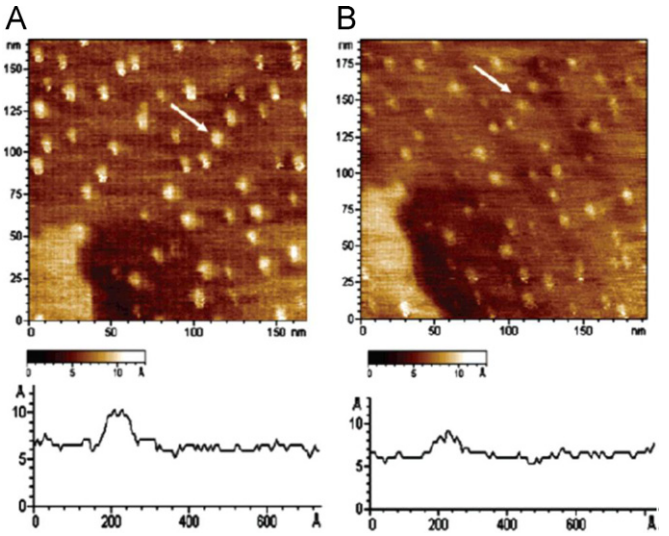

Fig. 4. EC-STM images of a cysteine mutant of PCSS adsorbed to a gold electrode polarized at 28 mV vs. SCE (A) and 222 mV vs. SCE (B). Height profiles for a single PCSS molecule (indicated by the arrows) are shown below the respective EC-STM images. Figure reproduced with permission from Bonanni et al., 2007.

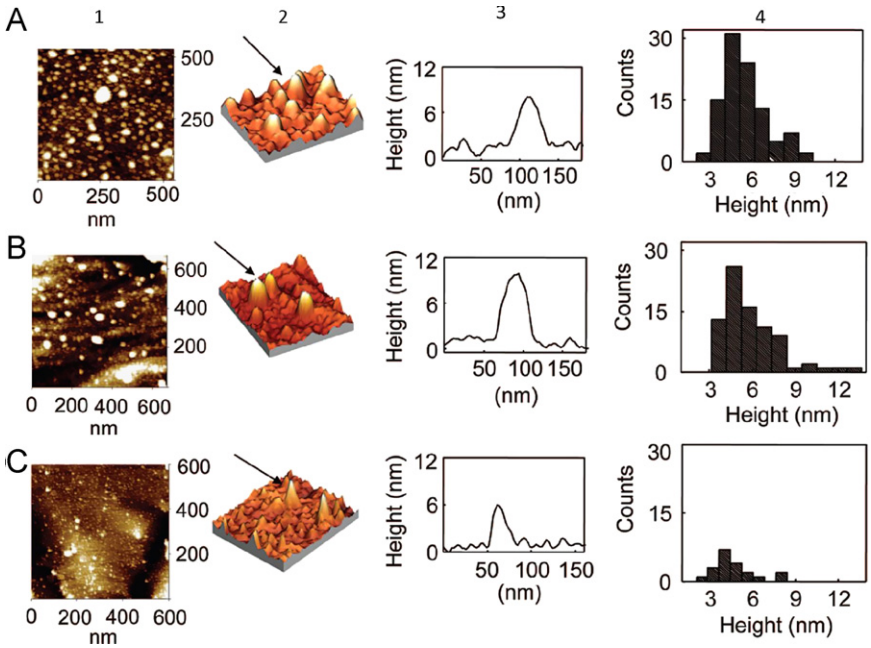

Fig. 5. TMAFM images of wild-type BMP (A), C156S (B), and C62S (C) covalently attached to a maleimide-functionalized SAM on a gold electrode. Column 1, 2D TMAFM images; Column 2, 3D TMAFM images, Column 3, height profiles for single enzyme molecules; Column 4, histograms of the molecular heights calculated for 100 individual enzyme molecules. Figure reproduced with permission from Ferrero et al., 2008.

linearity of the cholesterol response. In a more recent study, De Micheli and co-workers used MWCNT-modified screen-printed electrodes to create CYP biosensors from the drug-metabolizing CYPs 3A4, 2B4, and 2C9 (Cararra, et al., 2011). The authors compared the sensitivity of 3A4 biosensors made with bare or MWCNT electrodes to the drug cyclophosphamide and found that incorporation of the MWCNTs greatly enhanced the sensitivity of the sensor. In addition, a new mathematical model was developed to de-convolute the biosensor response from multiple drugs in a mixture, paving the way for detection of multiple drugs in human plasma samples.

Quantum dots and nanostructured gold are also being used to create novel CYP biosensors. Komatsu and co-workers discovered that the nanostructured surface of sputtered gold electrodes enhances the electroactivity of CYP3A4 adsorbed to the surface via a naphthalene thiolate SAM (Mie et al., 2010). Using these nanostructured gold electrodes, the authors measured an electron transfer rate constant of $340 \pm 40\ s^{-1}$ for electron transfer to 3A4. Substrate turnover was not assessed; however, a positive potential shift of the 3A4 redox potential in the presence of the 3A4 substrate testosterone suggested that the electrode-immobilized 3A4 was capable of substrate binding. In a follow-up study, the same research group examined the direct electrochemistry of 3A4 further by immobilizing 3A4 microsomes on gold nanodome arrays prepared by microfabrication (Ikegami et al., 2011). Gold nanodome arrays were generated using anodized aluminum foil as a template, and AFM images of nanodomes produced under optimal conditions revealed an organized array of nanostructures that were approximately 150 nm in diameter. Microsomes containing 3A4 were adsorbed onto a naphthalene thiolate SAM formed on the gold nanodomes, and aerobic CV scans of the nanodome-modified 3A4 electrode showed that the nanostructures led to an enhanced cathodic current when compared to a 3A4 electrode made using gold without nanostructures. A recent study by Ndangili et al. also examined the effects of a nanostructured surface on the direct electrochemistry of CYPs but used ZnSe quantum dots instead of gold nanodome arrays or gold nanoparticles (Ndangili et al., 2011). The authors used amine coupling to conjugate ZnSe quantum dots coated with an MPA SAM to a gold disk electrode modified with a cystamine SAM. Recombinant CYP3A4 was then amine-coupled to unreacted carboxyl groups on the immobilized ZnSe quantum dots to create a nanostructured 3A4 biosensor. The particle diameter of the MPA–ZnSe quantum dots was estimated from UV absorption to be 3.40 nm, much smaller than the gold nanodomes prepared in the aforementioned study. An aerobic CV scan of the Au/CYSAM/ZnSe/3A4 electrode revealed a reduction peak at -200 mV vs. Ag/AgCl while a more negative reduction potential was observed for a Au/CYSAM/3A4 electrode without quantum dots. This positive shift in the reduction potential with ZnSe quantum dots was attributed to the ability of quantum dots to confine electrons and thus lower the activation energy for electron transfer (Liu et al., 2006). The Au/CYSAM/ZnSe/3A4 electrode functioned as a biosensor for the detection of the hormone 17β-estradiol (E2); a plot of the current response as a function of E2 concentration followed Michaelis–Menten kinetics. Not surprisingly, the nanostructured electrode surface imparted by the ZnSe quantum dots enhanced the electrocatalytic response of the 3A4 biosensor to E2 (Fig. 6).

5. Concluding remarks

The future for CYP biosensors lies in the development of miniaturized systems made from nanostructured materials. Site-specific attachment and orientation of CYPs on the electrode surface is also gaining ground as a popular immobilization strategy due to the enhanced electroactivity that results when the enzyme is attached in a more productive orientation for electron transfer. Miniaturized systems, such as the microfluidic device recently developed by Gilardi and co-workers with CYP3A4 (Fantuzzi et al., 2010), may eventually lead to the development of portable CYP biosensor chips for diagnostic or clinical use. Nanostructured electrodes are gradually becoming the system of choice for the construction of CYP biosensors and it is likely there

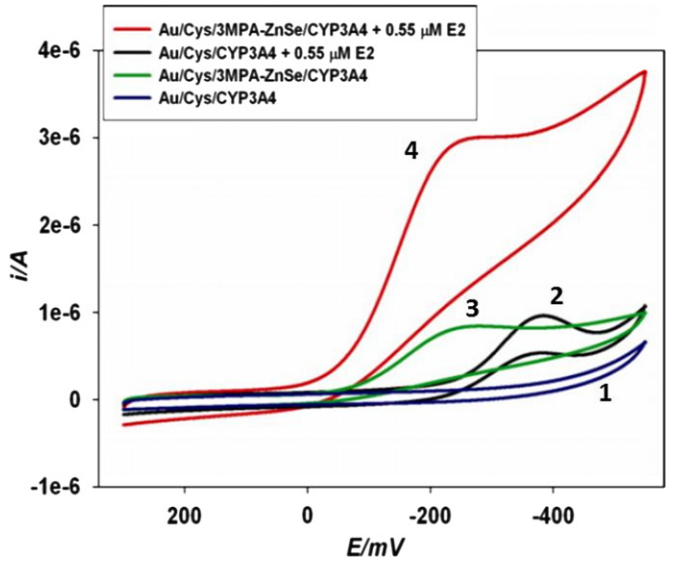

Fig. 6. Aerobic CVs recorded at a scan rate of 0.04 V/s using Au/Cys/CYP3A4 (curves 1 and 2) and Au/Cys/3MPA-ZnSe/CYP3A4 (curves 3 and 4) electrodes with (curves 2 and 4) and without (curves 1 and 3) 0.55 μM of the 3A4 substrate 17β-estradiol (E2) in KPi buffer at pH 7.4. All potentials are referenced to Ag/AgCl (3 M KCl). Figure reproduced with permission from Ndangili et al., 2011.

will be more examples of these systems in the future. Gold nanoparticles are especially attractive because they are easy to make, can be functionalized with various chemistries, and have been shown to serve as "excellent electron transfer relays" for the direct electrochemistry of enzymes (Jensen et al., 2007). Direct attachment of the buried CYP heme to the electrode also remains a possibility. This has already been accomplished for glucose oxidase biosensors (Zayats et al., 2002), although the direction of electron transfer occurs from the cofactor to the electrode as opposed to CYP biosensors where electron transfer occurs from the electrode to the cofactor. With the proper chemistry, this approach might be used in the future to directly wire CYPs to an electrode.

It is not yet clear if electrochemically-driven CYP catalysis mimics electron transfer and catalysis in vivo or even in solution. Many questions remain about the nature of electron transfer from the electrode to the buried P450 heme and what effects, if any, immobilization and/or direct electrochemistry has on the conformation of CYPs and the electronic environment of the heme. The discovery of inactive P420 in some electrode systems warrants rigorous surface characterization of CYP biosensors. Whether these issues are important for a given CYP biosensor remains unclear and may depend on the specific application. On the one hand, a CYP biosensor developed to serve as an initial screening tool for CYP reactivity of lead candidates in drug development may not need to duplicate exactly the enzyme's natural function as long as the relative ranking of compound activities follows that which occurs in vivo. On the other hand, a CYP biosensor designed to accurately replicate the human response—a so-called patient-on-a-chip—needs to behave identically to the corresponding in vivo system, in which case mimicking the natural mechanism of electron transfer to the CYP in its native conformation becomes paramount.

Acknowledgments

This work was supported by the National Science Foundation.

References

Alonso-Lomillo, M.A., Gonzalo-Ruiz, J., Domínguez-Renedo, O., Muñoz, F.J., Arcos-Martínez, M.J., 2008. Biosensors and Bioelectronics 23 (11), 1733–1737.
Anandan, V., Gangadharan, R., Zhang, G., 2009. Sensors 9 (3), 1295–1305.
Ansede, J.H., Thakker, D.R., 2004. Journal of Pharmaceutical Sciences 93 (2), 239–255.
Antonini, M., Ghisellini, P., Pastorino, L., Paternolli, C., Nicolini, C., 2003. IEE Proceedings of-Nanobiotechnology 150 (1), 31–34.
Asturias-Arribas, L., Alonso-Lomillo, M.A., Domínguez-Renedo, O., Arcos-Martínez, M.J., 2011. Analytica Chimica Acta 685 (1), 15–20.
Bistolas, N., Wollenberger, U., Jung, C., Scheller, F.W., 2005. Biosensors and Bioelectronics 20 (12), 2408–2423.
Bonanni, B., Andolfi, L., Bizzarri, A.R., Cannistraro, S., 2007. The Journal of Physical Chemistry B 111 (19), 5062–5075.
Bonifacio, A., Millo, D., Keizers, P.H.J., Boegschoten, R., Commandeur, J.N.M., Vermeulen, N.P.E., Gooijer, C., van der Zwan, G., 2008. Journal of Biological Inorganic Chemistry: JBIC: A Publication of the Society of Biological Inorganic Chemistry 13 (1), 85–96.
Carrara, S., Shumyantseva, V.V., Archakov, A.I., Samori, B., 2008. Biosensors and Bioelectronics 24 (1), 148–150.
Cararra, S., Cavallini, A., Erokhin, V., De Micheli, G., 2011. Biosensors and Bioelectronics 26 (9), 3914–3919.
Dai, C., Ding, Y., Li, M., Fei, J., 2012. Microchimica Acta 176 (3-4), 397–404.
Davis, J.J., Djuricic, D., Lo, K.K.W., Wallace, E.N.K., Wong, L., Hill, H.A.O., 2000. Faraday Discussions 116, 15–22.
Dodhia, V.R., Sassone, C., Fantuzzi, A., Di Nardo, G., Sadeghi, S.J., Gilardi, G., 2008. Electrochemistry Communications 10 (11), 1744–1747.
Estabrook, R.W., Faulkner, K.M., Seth, M.S., Fisher, C.W., 1996. Methods in Enzymology 272, 44–51.
Estavillo, C., Lu, Z., Jansson, I., Schenkman, J.B., Rusling, J.F., 2003. Biophysical Chemistry 104 (1), 291–296.
Fantuzzi, A., Fairhead, M., Gilardi, G., 2004. Journal of the American Chemical Society 126 (16), 5040–5041.
Fantuzzi, A., Capria, E., Mak, L.H., Dodhia, V.R., Sadeghi, S.J., Collins, S., 2010. Analytical Chemistry 82 (24), 10222–10227.
Ferroro, V.E.V., Andolfi, L., Di Nardo, G., Sadeghi, S.J., Fantuzzi, A., Cannistraro, S., Gilardi, G., 2008. Analytical Chemistry 80 (22), 8438–8446.
Fleming, B.D., Johnson, D.L., Bond, A.M., Martin, L.L., 2006. Expert Opinion on Drug Metabolism and Toxicology 2 (4), 581–589.
Hlavica, P., Schulze, J., Lewis, D.F.V., 2003. Journal of Inorganic Biochemistry 96 (2-3), 279–297.
Holtmann, D., Mangold, K., Schrader, J., 2009. Biotechnology Letters 31 (5), 765–770.
Hoa, Hui Bon, Di Primo, G., Dondaire, C., Sligar, I., Gunsalus, S., Douzou, P., I.C., 1989. Biochemistry 28 (2), 651–656.
Ikegami, M., Mie, Y., Hirano, Y., Suzuki, M., Komatsu, Y., 2011. Colloids and Surfaces A: Physicochemical and Engineering Aspects 384 (1-3), 388–392.
Imai, Y., Sato, R., 1967. European Journal of Biochemistry/FEBS 1 (4), 419–426.
Iwuoha, E.I., Kane, S., Anita, C.O., Smyth, M., Ortiz de Montellano, P.R., Fuhr, U., 2000. Electroanalysis 12 (12), 980–986.
Jensen, P.S., Chi, Q., Grumsen, F.B., Abad, J.M., Horsewell, A., Schiffrin, D.J., Ulstrup, J., 2007. Journal of Physical Chemistry C 111 (16), 6124–6132.
Johnson, D.L., Lewis, B.C., Elliot, D.J., Miners, J.O., Martin, L.L., 2005. Biochemical Pharmacology 69 (10), 1533–1541.
Johnson, D.L., Martin, L.L., 2005. Journal of the American Chemical Society 127 (7), 2018–2019.
Joseph, S., Rusling, J.F., Lvov, Y.M., Friedberg, T., Fuhr, U., 2003. Biochemical Pharmacology 65 (11), 1817–1826.
Kazlauskaite, J., Westlake, A.C.G., Wong, L., Hill, H.A.O., 1996. Chemical Communications 18, 2189–2190.
Krishnan, S., Wasalathanthri, D., Zhao, L., Schenkman, J.B., Rusling, J.F., 2011. Journal of the American Chemical Society 133 (5), 1459–1465.
Kumar, R.A., Clark, D.S., 2006. Current Opinion in Chemical Biology 10 (2), 162–268.
Lei, C., Wollenberger, U., Jung, C., Scheller, F.W., 2000. Biochemical and Biophysical Research Communications 268 (3), 740–744.
Lewis, D.F.V., Hlavica, P., 2000. Biochimica et Biophysica Acta 1460 (2-3), 353–374.
Liu, M., Shi, G., Zhang, L., Cheng, Y., Jin, L., 2006. Electrochemistry Communications 8 (2), 305–310.
Liu, S., Peng, L., Yang, X., Wu, Y., He, L., 2008. Analytical Biochemistry 375 (2), 209–216.
Lo, K.K., Wong, L., Hill, H.A.O., 1999. FEBS Letters 451 (3), 342–346.
Lvov, Y.M., Lu, Z., Schenkman, J., Zu, X., Rusling, J.F., 1998. Journal of the American Chemical Society 120 (17), 4073–4080.
Mak, L.H., Sadeghi, S.J., Fantuzzi, A., Gilardi, G., 2010. Analytical Chemistry 82 (12), 5357–5362.
Mhaske, S.D., Ray, M., Mazumdar, S., 2010. Inorganica Chimica Acta 363 (12), 2804–2811.
Mie, Y., Ikegami, M., Komatsu, Y., 2010. Electrochemistry Communications 12 (6) 860-683.
Mouro, C., Jung, C., Bondon, A., Simonneaux, G., 1997. Biochemistry 36 (26), 8125–8134.
Ndangili, P.M., Jijana, A.M., Baker, P.G.L., Iwuoha, E.I., 2011. Journal of Electroanalytical Chemistry 653 (1-2), 67–74.

Nikki, K., Gregory, B., 2003. Electrochemistry of redox-active protein films immobilized on self-assembled monolayers of organothiols. In: Rusling, James (Ed.), Surfactant Science Series. Biomolecular Films, 111. Marcel Dekker Inc., New York.
O'Keefe, D.H., Ebel, R.E., Peterson, J.A., Maxwell, J.C., Caughey, W.S., 1978. Biochemistry 17 (26), 5845–5852.
Omura, T., Sato, R., 1964. The Journal of Biological Chemistry 239 (7), 2370–2378.
Panicco, P., Astuti, Y., Fantuzzi, A., Durrant, J.R., Gilardi, G., 2008. The Journal of Physical Chemistry B 112 (44), 14063–14068.
Panicco, P., Dodhia, V.R., Fantuzzi, A., Gilardi, G., 2011. Analytical Chemistry 83 (6), 2179–2186.
Perera, R., Sono, M., Sigman, J.A., Pfister, T.D., Lu, Y., Dawson, J.H., 2003. Proceedings of the National Academy of Sciences, USA 100 (7), 3641–3646.
Reipa, V., Mayhew, M.P., Vilker, V., 1997. Proceedings of the National Academy of Sciences, USA 94 (25), 13554–13558.
Rhieu, S.Y., Ludwig, D.R., Siu, V.S., Palmore, G.T.R., 2009. Electrochemistry Communications 11 (10), 1857–1860.
Rudakov, Y.O., Shumyantseva, V.V., Bulko, T.V., Suprun, E.V., Kuznetsova, G.P., Samenkova, N.F., Archakov, A.I., 2008. Journal of Inorganic Biochemistry 102 (11), 2020–2025.
Sadeghi, S.J., Fantuzzi, A., Gilardi, G., 2011. Biochimica et Biophysica Acta 1814 (1), 237–248.
Shukla, A., Gillam, E.M., Mitchell, D.J., Bernhardt, P.V., 2005. Electrochemistry Communications 7 (4), 437–442.
Shumyantseva, V.V., Bulko, T.V., Usanov, S.A., Schmid, R.D., Nicolini, C., Archakov, A.I., 2001. Journal of Inorganic Biochemistry 87 (4), 185–190.
Shumyantseva, V.V., Ivanov, Y.D., Bistolas, N., Scheller, F.W., Archakov, A.I., Wollenberger, U., 2004. Analytical Chemistry 76 (20), 6046–6052.
Shumyantseva, V.V., Bulko, T.V., Archakov, A.I., 2005a. Journal of Inorganic Biochemistry 99 (5), 1051–1063.
Shumyantseva, V.V., Carrara, S., Bavastrello, V., Riley, J.D., Bulko, T.V., Skryabin, K.G., Archakov, A.I., Nicolini, C., 2005b. Biosensors and Bioelectronics 21 (1), 217–222.
Shumyantseva, V.V., Bulko, T.V., Rudakov, Y.O., Kuznetsova, G.P., Samenkova, N.F., Lisitsa, A.V., Karuzina, I.I., Archakov, A.I., 2007. Journal of Inorganic Biochemistry 101 (5), 859–865.
Shumyantseva, V.V., Bulko, T.V., Suprun, E.V., Chalenko, Y.M., Yu.Vagin, M., Rudakov, Y.O., Shatskaya, M.A., Archakov, A.I., 2011. Biochimica et Biophysica Acta 1814 (1), 94–101.
Sugihara, N., Ogoma, Y., Abe, K., Kondo, Y., Akaike, T., 1998. Polymers for Advanced Technology 9 (5), 307–313.
Sultana, N., Schenkman, J.B., Rusling, J.F., 2005. Journal of the American Chemical Society 127 (39), 13460–13461.
Tao, N.J., 1996. Physical Review Letters 76 (21), 4066–4069.
Todorovic, S., Jung, C., Hildebrandt, P., Murgida, D.H., 2006. Journal of Biological Inorganic Chemistry: JBIC: A Publication of the Society of Biological Inorganic Chemistry 11 (1), 119–127.
Traylor, M.J., Ryan, J.D., Arnon, E.S., Dordick, J.S., Clark, D.S., 2011. Journal of the American Chemical Society 133 (37), 14476–14479.
Trubetskoy, O.V., Gibson, J.R., Marks, B.D., 2005. Journal of Biomolecular Screening: The Official Journal of the Society for Biomolecular Screening 10 (1), 56–66.
Udit, A.K., Gray, H.B., 2005. Biochemical and Biophysical Research Communications 338 (1), 470–476.
Udit, A.K., Hagen, K.D., Goldman, P.J., Star, A., Gillan, J.M., Gray, H.B., Hill, M.G., 2006a. Journal of the American Chemical Society 128 (31), 10320–10325.
Udit, A.K., Hill, M.G., Gray, H.B., 2006b. Langmuir : the ACS Journal of Surfaces and Colloids 22 (25), 10854–10857.
Williams, J.A., Hyland, R., Jones, B.C., Smith, D.A., Hurst, S., Goosen, T.C., Peterkin, V., Koup, J.R., Ball, S.E., 2004. Drug Metabolism and Disposition: The Biological Fate of Chemicals 32 (11), 1201–1208.
Wu, Y., Liu, X., Zhang, L., Wang, C., 2011. Biosensors and Bioelectronics 26, 2177–2182.
Yang, M., Kabulski, J.L., Wollenberg, L., Chen, X., Subramanian, M., Tracy, T.S., Lederman, D., Gannett, P.M., Wu, N., 2009. Drug Metabolism and Disposition 37 (4), 892–899.
Yu, C.A., Gunsalus, I.C., 1974. The Journal of Biological Chemistry 249 (1), 102–106.
Zayats, M., Katz, E., Willner, I., 2002. Journal of the American Chemical Society 124 (7), 14724–14735.
Zhang, Z., Nassar, A.F., Lu, Z., Schenkman, J.B., Rusling, J.F., 1997. Faraday Transactions 93 (9), 1769–1774.
Zhukov, A.A., Archakov, A.I., 1985. Biochemistry (Moscow) 50, 1939–1952.